crystals

MDPI

Article

kHz, 10s TW, Femtosecond Source Based on Yb:YAG Thin Disk Laser Pumped OPCPA of Low Quantum Defect

Keyang Liu [1,†], Xin Liu [1,2,†], Jinhui Li [1,2], Hushan Wang [1,2], Yishan Wang [1,2], Wei Zhao [1,2], Huabao Cao [1,2,*] and Yuxi Fu [1,2,*]

[1] XIOPM Center for Attosecond Science and Technology, State Key Laboratory of Transient Optics and Photonics, Xi'an Institute of Optics and Precision Mechanics, Chinese Academy of Sciences, Xi'an 710119, China
[2] University of Chinese Academy of Sciences, Beijing 100049, China
* Correspondence: caohuabao@opt.ac.cn (H.C.); fuyuxi@opt.ac.cn (Y.F.)
† These authors contributed equally to this work.

Abstract: We propose to obtain kHz, 10s TW, femtosecond sources through optical parametric chirped pulse amplification (OPCPA) pumped by Yb:YAG thin disk lasers. The final amplifiers of the OPCPA are based on LGS ($LiGaS_2$) crystals with wide transparent range. To suppress the quantum defect for high efficiency, the final amplifiers are designed such that the wavelength of the signal is set very close to 1.03 μm, while the idler spectra span from 4–8 μm. Multiple crystals with different phase-matching configuration can be employed for the amplification of different spectral regions to support broadband pulse amplification. According to the numerical simulations, the pulse duration from Yb:YAG lasers can be shortened to 20–30 fs pulse with efficiency beyond 60%. This technique is energy scalable with the size of the LGS crystal size and can support a 26 TW pulse with current available LGS. The output pulses are ideal drivers for secondary light and particle source generation.

Keywords: Yb:YAG lasers; optical parametric chirped pulse amplification; low quantum defect

Citation: Liu, K.; Liu, X.; Li, J.; Wang, H.; Wang, Y.; Zhao, W.; Cao, H.; Fu, Y. kHz, 10s TW, Femtosecond Source Based on Yb:YAG Thin Disk Laser Pumped OPCPA of Low Quantum Defect. *Crystals* **2023**, *13*, 481. https://doi.org/10.3390/cryst13030481

Academic Editor: Vladimir Chvykov

Received: 14 February 2023
Revised: 26 February 2023
Accepted: 8 March 2023
Published: 10 March 2023

1. Introduction

Lasers with pulse duration of 10s fs combined with high pulse energy are essential for generating secondary light and particle sources, including terahertz and X-ray sources [1–3], high energy attosecond pulses [4–6], and plasma-based particle acceleration [7,8]. The fluxes of the secondary sources increase with average power of driving lasers, which is significant to decrease the experimental period and improve signal-to-noise ratios. Therefore, lasers with high average power, 10s fs pulse duration and high pulse energy are under intensive investigation. Currently, lasers based on coherent beam combination based on Yb doped fibers, Yb:YAG Inoslabs, room temperature and cryogenically cooled Yb:YAG thin-disks reaches kW class average power [9–12]. Among them, Yb:YAG thin-disk lasers are especially promising for serving as driving sources, which provide the highest pulse energy ranging from a few millijoule to Joule class up to now. However, the long pulse duration above several hundreds of fs hinders its applications, which is limited by the narrow emission bandwidth of the lasering materials.

To obtain light sources of 10s fs based on Yb:YAG lasers, a great amount of effort has been made from various groups to shorten the pulse duration through third order nonlinear process, namely the post-compression technologies, including techniques of multiple thin plates, multi-pass cell, and hollow-core fiber [13]. To date, the multiple thin plates technique has only been demonstrated for pulse shortening of lasers with mJ class energy [14]. In contrast, the gas-filled multi-pass cells and gas filled hollow-core fiber techniques have been applied to higher energy scenarios. For instance, the pulse duration was successfully shortened from 1.3 ps to 41 fs with pulse energy of approximately 18 mJ based on gas-filled multipass cell [15], and was shortened from 230 fs to 25 fs with pulse energy of 40 mJ

based on gas-filled hollow-core fiber [16]. Because of the quasi-waveguide and waveguide structure provided by the aforementioned post-compression techniques, decent beam quality can be obtained, i.e., high percentage of fundamental mode. Nevertheless, the energy of the pulse is limited by the critical power of self-focusing, the ionization threshold of the gas, and the damage threshold of the optics [17,18]. Thus, higher pulse energy demands much larger setup, which is impractical for most of the laboratories. Recently, pulse shortening of 112 mJ was achieved with 15 m long multipass cell, even with the help of donut transverse mode [19]. Much longer setup is needed when such a technique is used for Joule class lasers. Alternatively, a pulse shortening technique based on thin films applied for collimated beams has also been proposed and studied [20]. However, small-scale self-focusing plays a significant role in such technique, which limits the achievable B-integral [21]. Therefore, the shortening factor of the pulse duration is much smaller than the former three counterparts so far [22,23]. Besides, there is a common difficulty for all the post-compression techniques that the dispersion pre-compensation cannot be implemented because most of the spectral components do not exist before the post-compression setup. Hence, the compressed main peaks always accompanied by multiple side lobes or wide pedestal because of the residual high order dispersion.

Optical parametric chirped pulse amplification (OPCPA) is a prevalent technology to generate femtosecond pulses. OPCPA can support broadband amplification, possesses low thermal effects and great wavelength flexibility [24]. Meanwhile, the OPCPA can deliver pulses with high temporal contrast, which is demanded for interaction with solid targets. Typical OPCPA systems are optimized for either the shortest possible pulse duration [25–27], or for maximum wavelength tunability [28,29]. On the one hand, the signal wavelength is usually far away from the pump, so the quantum efficiency is quite low. On the other hand, the spatio-temporal shapes of the pulses are not super Gaussian for most cases, and uniform frequency conversion cannot be realized spatially and temporally, resulting in a large amount of residual pump energy.

In this work, we suggest OPCPA of low quantum defect served as an approach to obtain femtosecond sources from Yb:YAG thin disk lasers. In the final amplification stage of the OPCPA system, the idler is set to much longer wavelength compared to the signal to elevate the quantum efficiency. The spatio-temporal shape of the pump lasers is set to be super Gaussian to allow uniform energy extraction allover spatio-temporal domain. To provide broad enough gain spectra, the final amplification stage consisting of multiple sub-amplifiers with different phase-matching configurations are considered. The approach is numerically investigated, which shows that efficiency greater than 60% for the final amplifiers can be reached when the pulse duration of sub-20 fs is obtained with excellent energy scalability.

2. Modeling Method and Parameters

The OPCPA here is simulated with a 4D numerical code based on split-step Fourier method [30,31]. The dispersion, diffraction, and crystal anisotropy are all considered in this code, offering an accurate description of three wave mixing procedure. The nonlinear crystals are the key components of the optical parametrical amplifiers. The damage threshold, the transmission range, and the phase-matching property all need to be taken into account. After survey of the materials, LGS crystal is chosen here. Because of the big band gap, the crystal is durable with pumping of 1.03 μm based on Yb:YAG lasers. The transmission band of an uncoated LGS crystal with thickness of 2 mm spans from 0.33–11.6 μm as shown in Figure 1a, which is broad enough to cover all the interested spectra in this work [32–34]. The LGS has already been used to generate 7–9 μm mid-infrared pulse with pulse duration of around 100 fs, where the idler spectrum located close to the pump [35]. To achieve high quantum efficiency, we employ the opposite scenario, in which the signal spectrum is close to that of the pump while the idler spectrum moves far to the mid-infrared range. Figure 1b shows three Type-I phase-matching geometries at XZ plane with phase-matching angles of 51.2, 45.7, and 41.4 degrees, respectively. Correspondingly, the internal noncolinear angles

are 0, 1.5, and 2.2 degrees. The gain spectra are adjacent with each other to provide a wide spectrum amplification.

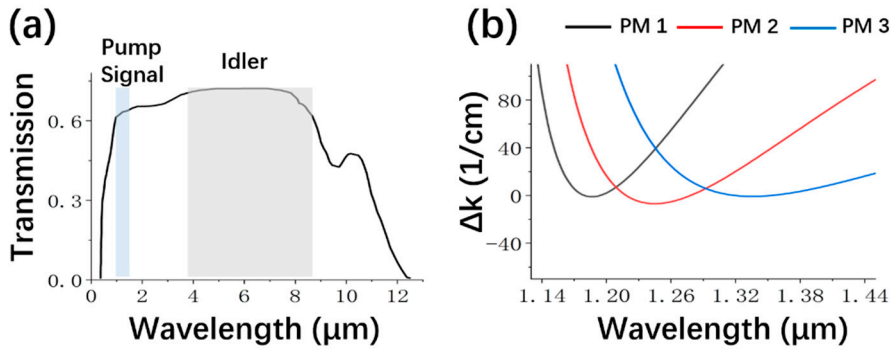

Figure 1. (**a**) The transmission range of LGS crystal, (**b**) three Type-I phase-matching geometries of LGS at XZ plane (PM1, PM2 and PM3 correspond to the phase matching angle 51.2, 45.7, 41.4 degrees and non-collinear angle 0, 1.5, 2.2 degrees respectively).

The suggested configuration of the final amplification state is shown in Figure 2a. The required broadband signal as shown in Figure 2b can be easily generated by OPCPA, since few cycle near-infrared pulses are routinely generated [36]. The final amplification stage consists of multiple amplification steps to sustain the bandwidth of the signal, as shown in Figure 2a. Two scenarios are studied here, i.e., two and three amplifiers as the final stage, to provide 30 fs and sub-20 fs pulses, respectively. The multiple pumps can either be sub-beams split from single laser or synchronized multiple lasers.

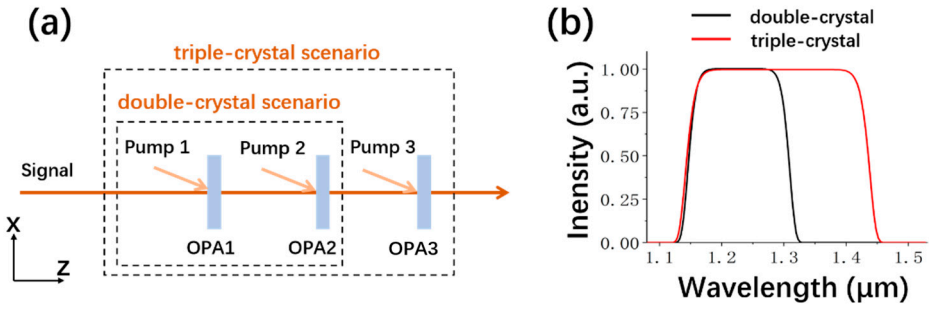

Figure 2. (**a**) The configurations of final amplifier of the OPCPA system for double-crystal scenario and triple-crystal scenario, (**b**) the super Gaussian signal spectrum of the two scenarios before amplification.

The energies of the signal and pump pulses of the final amplification stage considered here are 20 mJ and 200 mJ, respectively. The pump can be provided with current available Yb:YAG thin disk lasers, such as Dira200 from Trumpf scientific lasers [37]. The spatial shape of signal is super Gaussian of six orders to ensure the uniform energy extraction of the amplifiers. The spectral shape of the signal is also set to super Gaussian to obtain super Gaussian temporal shape after stretcher as showed in Figure 3a. Because the damage threshold of LGS for 1 ps pump is around 50 GW/cm^2 [35], the summation of the pump pulse durations is set to ~100 ps with the peak intensity of 5 GW/cm^2, which is below damage threshold of LGS according to the square root scaling law under different pulse durations [38]. With such pump intensity, gain around 10 is achievable for LGS with a few millimeters thickness. The spatial and temporal shapes of pumps are both 6 order super Gaussian. Flat-top beams have already been obtained for cryogenic cooled Yb:YAG thin disk lasers [12,39]. Flat-top pumps can also be obtained by beam shaping, which has already been demonstrated experimentally [40]. The super Gaussian temporal shape of the pump can be realized with the help of acousto-optic pulse shaping based on the fact that the pumps are chirped [41]. The other parameters of the OPAs are presented in Table 1.

The pulse durations and relative delays of the pumps are selected to effectively amplify the whole signal spectra.

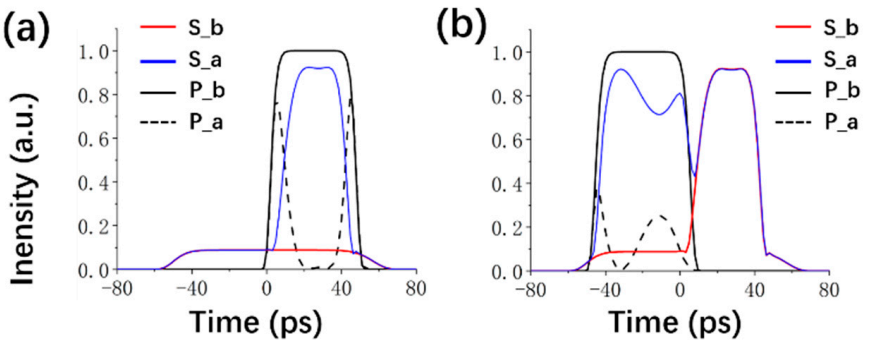

Figure 3. The evolution of the signal and pumps in the temporal domain (S: signal, P: pump, b: before amplification, a: after amplification, e.g., S_b means signal before amplification) for double-crystal scenario (**a**) OPA1 and (**b**) OPA2.

Table 1. The parameters of OPAs for double-crystal scenario and triple-crystal scenario.

Parameters	Double-Crystal Scenario		Triple-Crystal Scenario		
Amplifier	**OPA1**	**OPA2**	**OPA1**	**OPA2**	**OPA3**
Phase-matching angle (degree)	51.2	45.7	51.2	45.7	41.4
Internal noncollinear angle (degree)	0	1.5	0	1.5	2.2
Pump pulse duration (ps)	45	50	22	32	40
Pump delay (ps)	25	−20	37	12	−22
Pump energy (mJ)	91.7	101.9	44.8	65.2	81.5

3. Results and Discussion

Firstly, the double-crystal scenario is theoretical studied. The evolution of the signal and pumps in the temporal domain are shown in Figure 3a,b. The thickness of LGS crystals in both OPA1 and OPA2 is 4 mm to reach the saturation regime. In the OPA1, the trailing part of the signal is amplified and the output signal energy is 67.9 mJ. The pump energy at the central part is efficiently extracted. The efficiency at the wings is much lower because of the phase mismatch and smaller pump intensity. The leading part of the signal is amplified by the OPA2, and the output signal energy is 136.1 mJ. One can observe back-conversion of pump, which causes modulation of the signal (see the blue solid line in Figure 3b). The effective efficiency of this amplification stage reaches 60% (input signal energy is deducted).

The energy extraction is also examined in the spatial domain. The temporal distributions of the residual pump along X axis for OPA1 and OPA2 are shown in Figure 4a,b, respectively. Compared to OPA1, the residual pump intensity of OPA2 is asymmetric along the X axis because of the noncollinear phase-matching geometry.

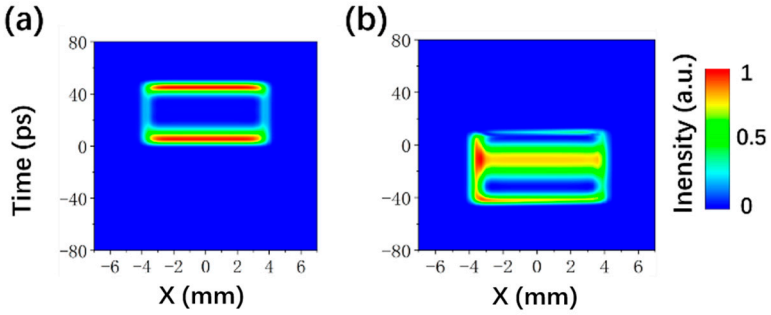

Figure 4. The temporal distributions of the residual pump along X axis for (**a**) OPA1 and (**b**) OPA2.

Figure 5a shows the amplified spectrum and the spectral phase after group delay dispersion (GDD) and third order dispersion (TOD) are compensated. The bandwidth is well maintained after the amplification stage with the pulse duration of 30.2 fs. The leaps of the spectral phases are induced by the optical parametrical phase of the amplifiers [42], which leads to multiple side lobes on both sides of the main peak, as shown by the black line in Figure 5b. After the residual high order dispersion is compensated, e.g., with Dazzler, the side lobes are effectively suppressed, as shown by the red solid line in Figure 5b. Hence, the peak intensity is about 1.30 times of the one before compensating the high order dispersion. The temporal distributions of the signal along X axis before and after the compensation of high order dispersion are shown in Figure 5c,d. No obvious spatio-temporal coupling presents, which guarantees good focusability of the signal pulse.

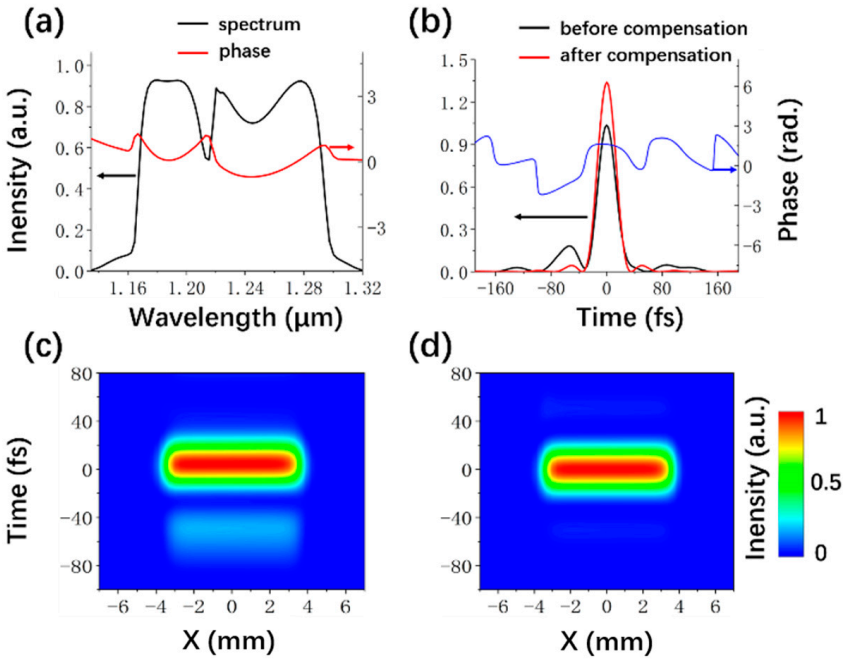

Figure 5. (**a**) The amplified spectrum and the spectral phase after dispersion compensation up to TOD for double-crystal scenario, (**b**) the temporal profiles of signal before and after the high order dispersion compensation, the temporal distributions of the signal along X axis (**c**) before and (**d**) after the compensation of the high order dispersion.

For the triple-crystal scenario, the evolution of the signal and pumps in the temporal domain are shown in Figure 6a–c. The thickness of the OPAs here is same as the double-crystal scenario. The output signal energies are 47.7 mJ, 88.9 mJ, and 140.3 mJ after each OPA. The effective efficiency of this amplification stage reaches 62.8%. The residual temporal distributions of the pump along X axis for the three OPAs are shown in Figure 6d–f, respectively.

The amplified spectrum and the spectral phase after dispersion compensated to TOD are shown in Figure 7a. The spectrum is broader than the double-crystal scenario, hence, the compressed pulse duration is 17.8 fs in this case. The side lobes are still visible because of the optical parametric phase [Figure 7b]. After the compensation of the high order dispersion, the peak intensity is increased to 1.28 times that of the original one. The temporal distributions of the signal along X axis before and after the compensation of high order dispersion are shown in Figure 7c,d and the spatiotemporal coupling is still negligible, similar to the double-crystal scenario.

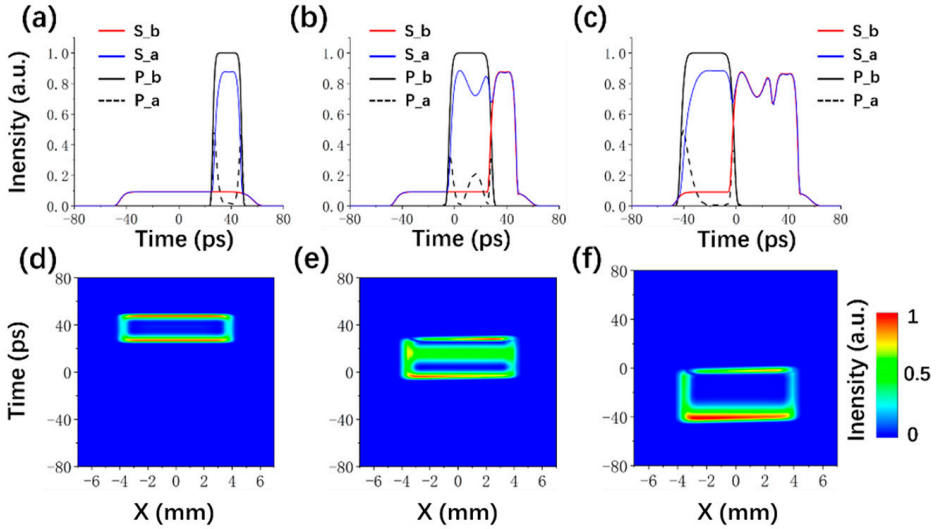

Figure 6. (**a**–**c**) The evolution of the signal and pumps in the temporal domain for triple-crystal scenario, (**d**–**f**) the temporal distributions of the residual pump along X axis for OPA1, OPA2 and OPA3, respectively.

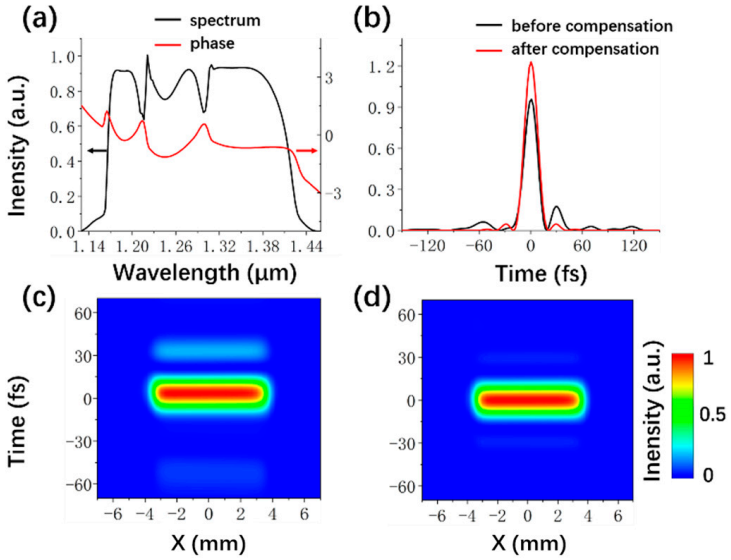

Figure 7. (**a**) The amplified spectrum and the spectral phase with dispersion compensation up to TOD for triple-crystal scenario, (**b**) the temporal profiles of signal before and after the residual high order dispersion is compensated, the temporal distributions of the signal along X axis (**c**) before and (**d**) after the compensation of the high order dispersion.

It is worth mentioning that the pulse duration can be further shortened with more OPAs designed for amplification of the spectral components towards longer wavelength. Nevertheless, it will increase the complexity of the system and decrease the overall efficiency due to higher quantum defects. Although the pump energy considered here is around 200 mJ, there is no obstacle to employing pumps with higher energy to promote the output pulse energy, except the limited size of LGS. At present, LGS with diameter of 20 mm can be obtained [32], which can support OPA pumped by 1.5 J. The amplified pulse can be compressed to transform a limited pulse duration by the compressor based on metal-multilayer dielectric gratings [43], and the total transmission can reach 88%. Hence, around 0.8 J can be achieved after compressor while assuming a conversion efficiency of 60% for the final amplification stages. This energy can support peak power above 40 TW at 1 kHz.

Because of the high repetition rate, the gratings of the compressor need active cooling for heat removal, which has already been demonstrated by LLNL [44].

4. Conclusions

We propose to employ low quantum defect OPCPA pumped by Yb:YAG thin disk lasers to develop kHz, 10s TW femtosecond sources. Compared to the conventional OPCPA, the signal wavelength is close to the pump. To suppress the spatio-temporal coupling, the pumps with the spatio-temporal shape of super Gaussian are employed. To support several 10s fs pulse duration, multiple crystals are employed for different spectral regions. When pumped with total energy of 200 mJ, 30 fs pulse duration is obtained with double-crystal scenario. The effective efficiency is 60%. The overall efficiency is bigger than 50%, taking into account the transmission of 88% for the compressor. The pulse duration can be further decreased with more OPAs. It is also energy scalable to above 40 TW class with kHz, Joule class pump, and employing currently available LGS crystal. This technique is promising to provide an approach for high repetition rate, high energy, thin disk Yb:YAG laser pulse shortening to ~20 fs, which is an effective driving source for the generation of various secondary sources.

Author Contributions: Conceptualization, H.C. and K.L.; methodology, K.L.; software, X.L. and J.L.; validation, X.L.; formal analysis, K.L. and X.L.; investigation, H.W.; resources, Y.W. and W.Z.; data curation, H.W. and J.L.; writing—original draft preparation, K.L. and X.L.; writing—review and editing, H.C. and Y.F.; funding acquisition, H.C. and Y.F. All authors have read and agreed to the published version of the manuscript.

Funding: This work was supported by National Natural Science Foundation of China (Nos. 62175256, 92050107, 61690222); Science and Technology Program of Xi'an (No. 202005YK01); Natural Science Basic Research Program of Shaanxi (No. 2019JCW-03); Major Science and Technology Infrastructure Pre-research Program of the CAS (No. J20-021-III); Key Deployment Research Program of XIOPM (No. S19-020-III); Innovation team in Shaanxi Province (No. E13311D301).

Data Availability Statement: The raw/processed data required to reproduce these findings cannot be shared at this time as the data also forms part of an ongoing study. However, they will be available from the corresponding author upon reasonable request.

Conflicts of Interest: The authors declare no conflict of interest.

References

1. Zhang, X.C.; Shkurinov, A.; Zhang, Y. Extreme terahertz science. *Nat. Photon.* **2017**, *11*, 16–18. [CrossRef]
2. Kramer, P.L.; Windeler, M.K.R.; Mecseki, K.; Champenois, E.G.; Hoffmann, M.C.; Tavella, F. Enabling high repetition rate nonlinear THz science with a kilowatt-class sub-100 fs laser source. *Opt. Express* **2020**, *28*, 16951–16967. [CrossRef]
3. Hädrich, S.; Rothhardt, J.; Krebs, M.; Demmler, S.; Klenke, A.; Tünnermann, A.; Limpert, J. Single-pass high harmonic gen-eration at high repetition rate and photon flux. *J. Phys. B At. Mol. Opt. Phys.* **2016**, *49*, 172002. [CrossRef]
4. Ferrari, F.; Calegari, F.; Lucchini, M.; Vozzi, C.; Stagira, S.; Sansone, G.; Nisoli, M. High-energy isolated attosecond pulses generated by above-saturation few-cycle fields. *Nat. Photon.* **2010**, *4*, 875–879. [CrossRef]
5. Wu, Y.; Cunningham, E.; Zang, H.; Li, J.; Chini, M.; Wang, X.; Wang, Y.; Zhao, K.; Chang, Z. Generation of high-flux atto-second extreme ultraviolet continuum with a 10 TW laser. *Appl. Phys. Lett.* **2013**, *102*, 201104. [CrossRef]
6. Fu, Y.; Yuan, H.; Midorikawa, K.; Lan, P.; Takahashi, E.J. Towards GW-scale isolated attosecond pulse far beyond carbon k-edge driven by mid-infrared waveform synthesizer. *Appl. Sci.* **2018**, *8*, 2451. [CrossRef]
7. Mangles, S.P.D.; Murphy, C.D.; Najmudin, Z.; Thomas, A.G.R.; Collier, J.L.; Dangor, A.E.; Divall, E.J.; Foster, P.S.; Gallacher, J.G.; Hooker, C.J.; et al. Monoenergetic beams of relativistic electrons from intense laser-plasma interactions. *Nature* **2004**, *431*, 535–538. [CrossRef]
8. Ouillé, M.; Vernier, A.; Böhle, F.; Bocoum, M.; Jullien, A.; Lozano, M.; Rousseau, J.-P.; Cheng, Z.; Gustas, D.; Blumenstein, A.; et al. Relativistic-intensity near-single-cycle light waveforms at kHz repetition rate. *Light Sci. Appl.* **2020**, *9*, 47. [CrossRef]
9. Schulz, M.; Riedel, R.; Willner, A.; Mans, T.; Schnitzler, C.; Russbueldt, P.; Dolkemeyer, J.; Seise, E.; Gottschall, T.; Hädrich, S.; et al. Yb: YAG innoslab amplifier: Efficient high repetition rate subpicosecond pumping system for optical parametric chirped pulse amplification. *Opt. Lett.* **2011**, *36*, 2456–2458. [CrossRef]
10. Nubbemeyer, T.; Kaumanns, M.; Ueffing, M.; Gorjan, M.; Alismail, A.; Fattahi, H.; Brons, J.; Pronin, O.; Barros, H.G.; Major, Z.; et al. 1 kW, 200 mJ picosecond thin-disk laser system. *Opt. Lett.* **2017**, *42*, 1381–1384. [CrossRef]

11. Herkommer, C.; Krötz, P.; Jung, R.; Klingebiel, S.; Wandt, C.; Bessing, R.; Walch, P.; Produit, T.; Michel, K.; Bauer, D.; et al. Ultrafast thin-disk multipass amplifier with 720 mJ operating at kilohertz repetition rate for applications in atmospheric research. *Opt. Express* **2020**, *28*, 30164–30173. [CrossRef] [PubMed]
12. Wang, Y.; Chi, H.; Baumgarten, C.; Dehne, K.; Meadows, A.R.; Davenport, A.; Murray, G.; Reagan, B.A.; Menoni, C.S.; Rocca, J.J. 1.1 J Yb: YAG picosecond laser at 1 kHz repetition rate. *Opt. Lett.* **2020**, *45*, 6615–6618. [CrossRef] [PubMed]
13. Seidel, M.; Balla, P.; Li, C.; Arisholm, G.; Winkelmann, L.; Hartl, I.; Heyl, C.M. Factor 30 pulse compression by hybrid multipass multiplate spectral broadening. *Ultrafast Sci.* **2022**, *2022*, 9754919. [CrossRef]
14. Lu, C.-H.; Wu, W.-H.; Kuo, S.-H.; Guo, J.-Y.; Chen, M.-C.; Yang, S.-D.; Kung, A.H. Greater than 50 times compression of 1030 nm Yb: KGW laser pulses to single-cycle duration. *Opt. Express* **2019**, *27*, 15638–15648. [CrossRef]
15. Kaumanns, M.; Pervak, V.; Kormin, D.; Leshchenko, V.; Kessel, A.; Ueffing, M.; Chen, Y.; Nubbemeyer, T. Multipass spectral broadening of 18 mJ pulses compressible from 1.3 ps to 41 fs. *Opt. Lett.* **2018**, *43*, 5877–5880. [CrossRef]
16. Fan, G.; Carpeggiani, P.A.; Tao, Z.; Coccia, G.; Safaei, R.; Kaksis, E.; Pugzlys, A.; Légaré, F.; Schmidt, B.E.; Baltuška, A. 70 mJ nonlinear compression and scaling route for an Yb amplifier using large-core hollow fibers. *Opt. Lett.* **2021**, *46*, 896–899. [CrossRef]
17. Böhle, F.; Kretschmar, M.; Jullien, A.; Kovacs, M.; Miranda, M.; Romero, R.; Crespo, H.; Morgner, U.; Simon, P.; Martens, R.L.; et al. Compression of CEP-stable multi-mJ laser pulses down to 4 fs in long hollow fibers. *Laser Phys. Lett.* **2014**, *11*, 095401. [CrossRef]
18. Hanna, M.; Délen, X.; Lavenu, L.; Guichard, F.; Zaouter, Y.; Druon, F.; Georges, P. Nonlinear temporal compression in multipass cells: Theory. *J. Opt. Soc. Am. B* **2017**, *34*, 1340–1347. [CrossRef]
19. Kaumanns, M.; Kormin, D.; Nubbemeyer, T.; Pervak, V.; Karsch, S. Spectral broadening of 112 mJ, 1.3 ps pulses at 5 kHz in a LG10 multipass cell with compressibility to 37 fs. *Opt. Lett.* **2021**, *46*, 929–932. [CrossRef]
20. Mourou, G.; Mironov, S.; Khazanov, E.; Sergeev, A. Single cycle thin film compressor opening the door to Zeptosec-ond-Exawatt physics. *Eur. Phys. J. Spec. Top.* **2014**, *223*, 1181–1188. [CrossRef]
21. Bespalov, V.I.; Talanov, V.I. Filamentary structure of light beams in nonlinear liquids. *J. Exp. Theoretical Phys. Lett.* **1966**, *3*, 307–310.
22. Mironov, S.Y.; Fourmaux, S.; Lassonde, P.; Ginzburg, V.N.; Payeur, S.; Kieffer, J.-C.; Khazanov, E.A.; Mourou, G. Thin plate compression of a sub-petawatt Ti:Sa laser pulses. *Appl. Phys. Lett.* **2020**, *116*, 241101. [CrossRef]
23. Ginzburg, V.; Yakovlev, I.; Kochetkov, A.; Kuzmin, A.; Mironov, S.; Shaikin, I.; Shaykin, A.; Khazanov, E. 11 fs, 1.5 PW laser with nonlinear pulse compression. *Opt. Express* **2021**, *29*, 28297. [CrossRef]
24. Butkus, R.; Danielius, R.; Dubietis, A.; Piskarskas, A.; Stabinis, A. Progress in chirped pulse optical parametric amplifiers. *Appl. Phys. B Laser Opt.* **2004**, *79*, 693–700. [CrossRef]
25. Yin, Y.; Chew, A.; Ren, X.; Li, J.; Wang, Y.; Wu, Y.; Chang, Z. Towards terawatt sub-cycle long-wave infrared pulses via chirped optical parametric amplification and indirect pulse shaping. *Sci. Rep.* **2017**, *7*, srep45794. [CrossRef]
26. Kessel, A.; Leshchenko, V.E.; Jahn, O.; Krüger, M.; Münzer, A.; Schwarz, A.; Pervak, V.; Trubetskov, M.; Trushin, S.A.; Krausz, F.; et al. Relativistic few-cycle pulses with high contrast from picosecond-pumped OPCPA. *Optica* **2018**, *5*, 434–442. [CrossRef]
27. Xue, B.; Tamaru, Y.; Fu, Y.; Yuan, H.; Lan, P.; Mücke, O.D.; Suda, A.; Midorikawa, K.; Takahashi, E.J. A custom-tailored multi-TW optical electric field for gigawatt soft-X-ray isolated attosecond pulses. *Ultrafast Sci.* **2021**, *2021*, 9828026. [CrossRef]
28. Migal, E.A.; Potemkin, F.; Gordienko, V.M. Highly efficient optical parametric amplifier tunable from near- to mid-IR for driving extreme nonlinear optics in solids. *Opt. Lett.* **2017**, *42*, 5218–5221. [CrossRef] [PubMed]
29. Musheghyan, M.; Geetha, P.P.; Faccialà, D.; Pusala, A.; Crippa, G.; Campolo, A.; Ciriolo, A.G.; Devetta, M.; Assion, A.; Manzoni, C.; et al. Tunable, few-cycle, CEP-stable mid-IR optical parametric amplifier for strong field applications. *J. Phys. B At. Mol. Opt. Phys.* **2020**, *53*, 185402. [CrossRef]
30. Andrianov, A.; Szabo, A.; Sergeev, A.; Kim, A.; Chvykov, V.; Kalashnikov, M. Computationally efficient method for Fourier transform of highly chirped pulses for laser and parametric amplifier modeling. *Opt. Express* **2016**, *24*, 25974–25982. [CrossRef]
31. Cao, H.; Tóth, S.; Kalashnikov, M.; Chvykov, V.; Osvay, K. Highly efficient, cascaded extraction optical parametric amplifier. *Opt. Express* **2018**, *26*, 7516–7527. [CrossRef] [PubMed]
32. Yelisseyev, A.; Lin, Z.S.; Starikova, M.; Isaenko, L.; Lobanov, S. Optical transitions due to native defects in nonlinear optical crystals $LiGaS_2$. *J. Appl. Phys.* **2012**, *111*, 113507. [CrossRef]
33. Isaenko, L.; Yelisseyev, A.; Lobanov, S.; Titov, A.; Petrov, V.; Zondy, J.-J.; Krinitsin, P.; Merkulov, A.; Vedenyapin, V.; Smirnova, J. Growth and properties of $LiGaX_2$ (X = S, Se, Te) single crystals for nonlinear optical applications in the mid-IR. *Cryst. Res. Technol.* **2003**, *38*, 379–387. [CrossRef]
34. Namboodiri, M.; Luo, C.; Indorf, G.; Golz, T.; Grguraš, I.; Buss, J.H.; Schulz, M.; Riedel, R.; Prandolini, M.J.; Laarmann, T. Optical properties of Li-based nonlinear crystals for high power mid-IR OPCPA pumped at 1 µm under realistic operational conditions. *Opt. Mater. Express* **2021**, *11*, 231–239. [CrossRef]
35. Qu, S.Z.; Liang, H.K.; Liu, K.; Zou, X.; Li, W.k.; Wang, Q.J.; Zhang, Y. 9 µm few-cycle optical parametric chirped-pulse amplifier based on $LiGaS_2$. *Opt. Lett.* **2019**, *44*, 2422–2425. [CrossRef] [PubMed]
36. Hrisafov, S.; Pupeikis, J.; Chevreuil, P.-A.; Brunner, F.; Phillips, C.; Gallmann, L.; Keller, U. High-power few-cycle near-infrared OPCPA for soft X-ray generation at 100 kHz. *Opt. Express* **2020**, *28*, 40145–40154. [CrossRef]
37. Product Dira Series Page of TRUMPF Scientific Lasers. Available online: https://www.trumpf-scientific-lasers.com/products/dira-series/ (accessed on 13 February 2023).
38. Wood, R.M. *Laser Damage in Optical Materials*; Taylor & Francis: Oxfordshire, UK, 2003; Chapter 4.

39. Zapata, L.E.; Lin, H.; Calendron, A.-L.; Cankaya, H.; Hemmer, M.; Reichert, F.; Huang, W.R.; Granados, E.; Hong, K.-H.; Kärtner, F.X. Cryogenic Yb: YAG composite-thin-disk for high energy and average power amplifiers. *Opt. Lett.* **2015**, *40*, 2610–2613. [CrossRef]
40. Zou, X.; Li, W.; Qu, S.; Liu, K.; Li, H.; Wang, Q.; Zhang, Y.; Liang, H. Flat-top pumped multi-millijoule mid-infrared parametric chirped-pulse amplifier at 10 kHz repetition rate. *Laser Photonics Rev.* **2021**, *15*, 2000292. [CrossRef]
41. Molchanov, V.Y.; Yushkov, K.B.; Kostryukov, P.V.; Gornostaev, P.B.; Vorobiev, N.S. Measurement of amplified binary-modulated chirped laser pulses generated by different acousto-optic pulse shaping algorithms. *Opt. Laser Technol.* **2021**, *142*, 107220. [CrossRef]
42. Wang, Y.; Wang, J.; Zhou, B.; Ma, J.; Yuan, P.; Qian, L. Spatiotemporal couplings through a nonlinear phase in broadband optical parametric amplification. *Opt. Lett.* **2021**, *46*, 5743–5746. [CrossRef]
43. Wang, J.; Jin, Y.; Ma, J.; Sun, T.; Jing, X. Design and analysis of broadband high-efficiency pulse compression gratings. *Appl. Opt.* **2010**, *49*, 2969–2978. [CrossRef] [PubMed]
44. Alessi, D.A.; Rosso, P.A.; Nguyen, H.T.; Aasen, M.D.; Britten, J.A.; Haefner, C. Active cooling of pulse compression diffraction gratings for high energy, high average power ultrafast lasers. *Opt. Express* **2016**, *24*, 30015–30023. [CrossRef] [PubMed]